

# Collective flow in 2.76 and 5.02 A TeV Pb + Pb collisions

Wenbin Zhao<sup>1</sup>, Hao-jie Xu<sup>1</sup>, Huichao Song<sup>1,2,3,a</sup> <sup>1</sup> Department of Physics and State Key Laboratory of Nuclear Physics and Technology, Peking University, Beijing 100871, China<sup>2</sup> Collaborative Innovation Center of Quantum Matter, Beijing 100871, China<sup>3</sup> Center for High Energy Physics, Peking University, Beijing 100871, China

Received: 2 April 2017 / Accepted: 2 September 2017 / Published online: 25 September 2017

© The Author(s) 2017. This article is an open access publication

**Abstract** In this paper, we study and predict flow observables in 2.76 and 5.02 A TeV Pb + Pb collisions, using the iEBE-VISHNU hybrid model with TRENTO and AMPT initial conditions and with different forms of the QGP transport coefficients. With properly chosen and tuned parameter sets, our model calculations can nicely describe various flow observables in 2.76 A TeV Pb + Pb collisions, as well as the measured flow harmonics of all charged hadrons in 5.02 A TeV Pb + Pb collisions. We also predict other flow observables, including  $v_n(p_T)$  of identified particles, event-by-event  $v_n$  distributions, event-plane correlations, (normalized) symmetric cumulants, non-linear response coefficients and  $p_T$ -dependent factorization ratios, in 5.02 A TeV Pb + Pb collisions. We find many of these observables to remain approximately the same values as the ones in 2.76 A TeV Pb + Pb collisions. Our theoretical studies and predictions could shed light to the experimental investigations in the near future.

## 1 Introduction

At extremely high temperature and density, the nuclear matter can experience a phase transition and form the quark–gluon plasma (QGP). The main goals of the relativistic heavy-ion collisions at Relativistic Heavy Ion Collider (RHIC) and the Large Hadron Collider (LHC) are to create the QGP and to explore its properties [1–9]. Since the running of RHIC in 2000, strong evidence has been accumulated for the creation of the QGP, including jet quenching, strong collective flow and the valence quark scaling of the elliptic flow [1,5–9]. Hydrodynamics and hybrid models are successful tools to simulate the collective expansion of the QGP fireball and to study various flow observables at RHIC and the LHC [10–15]. The past research has revealed that the created QGP fire-

balls fluctuate event-by-event and behave like nearly perfect liquids with very small specific shear viscosity [13–19].

In the past few years, various flow observables have been extensively measured and studied in 2.76 A TeV Pb + Pb collisions, including the integrated and differential flow harmonics [20–27], the event-by-event  $v_n$  distributions [27–30], the event-plane correlations [31–35], the correlations between different flow harmonics (symmetric cumulants) [35–41], the  $p_T$ - and  $\eta$ -dependent de-correlations of the flow vector [42–49], etc. Many of these flow observables reflect the information on the event-by-event initial state fluctuations and the non-linear evolution of the system, which provide constraints for the initial condition models and the QGP transport coefficients. For example, it was found that the event-by-event  $v_n$  distributions mostly follow the event-by-event  $\varepsilon_n$  distributions of the initial state for  $n = 2$  and 3, which does not favor the traditional MC-Glauber and MC-KLN models with nucleon position fluctuations [27,28]. Based on eikonal entropy deposition via a reduced thickness function, Moreland et al. constructed a parametric TRENTO model that could match various initial conditions with tunable parameters [50]. Using TRENTO initial conditions, the Duke and OSU group has performed massive data simulations of iEBE-VISHNU hybrid model and systematically evaluated the measured multiplicity, mean  $p_T$  and integrated  $v_n$  in 2.76 A TeV Pb + Pb collisions. Their simulations extracted a temperature-dependent specific shear viscosity  $\eta/s(T)$ , which is an approximately linear function with a minimum value close to the KSS bound near  $T_c$  [51]. The early hydrodynamic and hybrid model simulations, using IP-Glasma [27], AMPT [26] or EKRT initial conditions [38], can also nicely fit the integrated and differential flow harmonics with a constant or temperature-dependent  $\eta/s$ , close to the KSS bound near  $T_c$ . In fact, the flow harmonics  $v_n$  are not sensitive to the details of the initial condition models as long as balanced initial eccentricities can be generated with some tunable parameters. Other flow measurements, e.g., the event-plane correlations, symmetric cumu-

<sup>a</sup> e-mail: [Huichaosong@pku.edu.cn](mailto:Huichaosong@pku.edu.cn)

lants, non-linear response coefficients, the de-correlation of the flow vector, etc., could reveal more details on initial state fluctuations and the non-linear hydrodynamic response [31–49]. A systematic study of these flow observables will help us to test the model calculations and the extracted QGP viscosity as well as to further constrain the initial condition models.

Recently, the ALICE collaboration has measured the integrated and differential flow harmonics of all charged hadrons in 5.02 A TeV Pb + Pb collisions [52]. It was found, with the collision energies raised from 2.76 to 5.02 A TeV,  $v_2$ ,  $v_3$  and  $v_4$  slightly increase with the increase of average transverse momentum, which is qualitatively agree with the early hydrodynamic predictions [53,54]. In this paper, we implement iEBE-VIHSNU hybrid model with TRENTO and AMPT initial conditions to study and predict various flow observables in 2.76 and 5.02 A TeV Pb + Pb collisions. We will use the available data of total multiplicities,  $p_T$  spectra of identified hadrons, and the integrated flow harmonics  $v_n$  of all charged hadrons to fix the free parameters in iEBE-VIHSNU simulations and then make predictions for other flow observables, including the differential flow harmonics  $v_n(p_T)$  of identified hadrons, the event-by-event  $v_n$  distributions, the event-plane correlations, the symmetric cumulants, non-linear response coefficients and the  $p_T$ -dependent factorization ratios. We have noticed that the McGill group also predicted various flow observables in 5.02 A TeV Pb + Pb collisions, using MUSIC simulations with the IP-Glasma initial conditions [55]. Compared with their calculations [55] and other early investigations [53,54], our predictions are more complete; they are also on time and can be measured in the near future. For example, the symmetric cumulants and non-linear response coefficients in 5.02 A TeV Pb + Pb collisions are for the first time predicted in this paper, which has not been done elsewhere as far as we know. Besides, the parameters in iEBE-VIHSNU are fine tuned to fit the published soft hadron data, which give more reliable predictions for these un-measured flow observables. For example, our descriptions of  $v_n(p_T)$  of all charged hadrons are better than the ones in [55]. Correspondingly, the predicted flow harmonics of identified hadrons are more reliable. Furthermore, it is worthwhile to investigate the same flow observables using the hydrodynamic calculations with different initial conditions, which could help us to understand the details of the initial state fluctuations and may help us to identify some flow observables to further constrains the initial conditions.

This paper is organized as the following: Sect. 2 introduces the iEBE-VIHSNU hybrid model and the set-ups of calculations with TRENTO and AMPT initial conditions. Section 3 introduces the methodology to calculate various flow observables. Section 4 presents and discusses the calculated and predicted flow observables in 2.76 and 5.02 A TeV Pb + Pb collisions. Section 5 summarizes and concludes this paper.

## 2 The model and set-ups of the calculations

### 2.1 iEBE-VISHNU hybrid model

iEBE-VISHNU [56] is an event-by-event version of the VISHNU hybrid model [57], which combines (2+1)-d viscous hydrodynamics VISH2+1 [58–60] to describe the expansion of the QGP fireball with a hadron cascade model (UrQMD) [61,62] to simulate the evolution of the hadronic matter.

In the hydrodynamics part, iEBE-VISHNU solves the transport equations for energy-momentum tensor  $T^{\mu\nu}$  and the second order Israel–Stewart equations for shear stress tensor  $\pi^{\mu\nu}$  and bulk pressure  $\Pi$  [58–60]:

$$\begin{aligned} \partial_\mu T^{\mu\nu}(x) &= 0, \quad T^{\mu\nu} = e u^\mu u^\nu - (p + \Pi) \Delta^{\mu\nu} + \pi^{\mu\nu}, \\ \dot{\Pi} &= -\frac{1}{\tau_\Pi} \left[ \Pi + \zeta \theta + \Pi \zeta T \partial_\mu \left( \frac{\tau_\Pi u^\mu}{2\zeta T} \right) \right], \\ \Delta^{\mu\alpha} \Delta^{\nu\beta} \dot{\pi}_{\alpha\beta} &= -\frac{1}{\tau_\pi} \\ &\quad \times \left[ \pi^{\mu\nu} - 2\eta \nabla^{(\mu} u^{\nu)} + \pi^{\mu\nu} \eta T \partial_\alpha \left( \frac{\tau_\pi u^\alpha}{2\eta T} \right) \right], \end{aligned} \quad (1)$$

where  $e$ ,  $p$  and  $T$  are the local energy density, pressure and temperature, and  $u^\mu$  is the flow 4-velocity.  $\Delta^{\mu\nu} = g^{\mu\nu} - u^\mu u^\nu$ ,  $\nabla^{(\mu} u^{\nu)} = \frac{1}{2}(\nabla^\mu u^\nu + \nabla^\nu u^\mu) - \frac{1}{3}\Delta^{\mu\nu}\partial_\alpha u^\alpha$  and  $\theta = \partial \cdot u$ .  $\eta$  is the shear viscosity,  $\zeta$  is the bulk viscosity, and  $\tau_\pi$ ,  $\tau_\Pi$  are the corresponding relaxation times. Here, we neglect the equations for net charge current and heat flow since we focus on the soft physics at the LHC, where both net baryon density and heat conductivity are negligible. With the Bjorken approximation,  $v_z = z/t$  [63], the above equations can be written in a 2+1-d form with longitudinal boost invariance [59,60,64], which largely increases the numerical efficiency compared with full 3+1-d simulations.

For the hydrodynamic simulations, one needs to input an equation of state (EoS),  $P = P(e)$ , to close the system. Following [51], we implement a state-of-art EoS that matches the recent lattice EoS at zero baryon density from the HotQCD collaboration [65] and the hadron resonance gas EoS using a smooth interpolation function.

In the hybrid model, the switch between hydrodynamics and hadron cascade simulations is realized by a particle event generator, which converts the hydrodynamic outputs on a switching hyper-surface into various hadrons with specific momentum and position for the succeeding UrQMD simulations. More specifically, such Monte Carlo event generator is constructed according to the differential Cooper–Frye formula [57]:

$$E \frac{d^3 N_i}{d^3 p}(x) = \frac{g_i}{(2\pi)^3} p \cdot d^3 \sigma(x) f_i(x, p), \quad (2)$$

where  $f_i$  is the distribution function of particle  $i$  which includes both equilibrium and non-equilibrium contributions  $f_i = f_{i0} + \delta f_i$ .  $d^3\sigma(x)$  is a volume element of the switching hyper-surface  $\Sigma$ , which is generally defined by a constant switching temperature  $T_{\text{switch}}$ . Following [51],  $T_{\text{switch}}$  is set to 148 MeV and the non-equilibrium distribution function has taken the form of  $\delta f = \delta f_{\text{shear}} = f_0(1 \mp f_0) \frac{p^\mu p^\nu \pi_{\mu\nu}}{2T^2(e+p)}$ .<sup>1</sup>

After the fluid has been converted into various hadrons, the evolution of the hadron matter is simulated by the ultra-relativistic quantum molecular dynamics (UrQMD) through solving the Boltzmann equations [61, 62]:

$$\frac{df_i(x, p)}{dt} = C_i(x, p), \tag{3}$$

where  $f_i(x, p)$  is the distribution function of hadron species  $i$  and  $C_i(x, p)$  is the corresponding collision term. According to these equations, the produced hadrons propagate along classical trajectories, together with the elastic, inelastic scatterings and resonance decays. When all the interactions cease, the evolution stops and the final information of produced hadrons is output to be further analyzed and compared with the experimental data.

### 2.2 Set-ups

In this paper, we implement two different initial conditions, called TRENTO and AMPT, in the iEBE-VISHNU simulations. In this sub-section, we will briefly introduce these two initial conditions and the set-ups of related parameters for the simulations in Pb + Pb collisions at 2.76 and 5.02 A TeV.

The TRENTO model parameterizes the initial entropy density via the reduced thickness function [50]:

$$s = s_0 \left( \frac{\tilde{T}_A^p + \tilde{T}_B^p}{2} \right)^{1/p}, \tag{4}$$

where  $\tilde{T}(x, y)$  is the modified participant thickness function  $\tilde{T}(x, y) = \sum_{i=1}^{N_{\text{part}}} \gamma_i T_p(x - x_i, y - y_i)$  and  $\gamma_i$  is a random weighting factor.  $T_p$  is the nucleon thickness function with a Gaussian form:  $T_p(x, y) = \frac{1}{2\pi w^2} \exp(-\frac{x^2+y^2}{2w^2})$  and  $w$  is a tunable effective nucleon width.  $s_0$  is a normalization factor and  $p$  is a tunable parameter, which makes TRENTO model

<sup>1</sup> Note that the bulk viscous correction  $\delta f_{\text{bulk}}$  is neglected here. In fact,  $\delta f_{\text{bulk}}$  has a variety of forms, which more or less influences the flow observables when bulk pressure or transverse momentum become large [66, 67]. To avoid such uncertainties for the massive data fitting, Ref. [51] directly set  $\delta f_{\text{bulk}} = 0$  in the particle event generator of iEBE-VISHNU. For our simulations with TRENTO initial condition, we input the same parameterizations for specific shear and bulk viscosity (para-I in Fig. 1) and thus set  $\delta f = \delta f_{\text{shear}}$  as [51]. For the AMPT initial condition, we input a constant specific shear viscosity and zero bulk viscosity (para-II in Fig. 1) in the iEBE-VISHNU simulations, which does not need the additional  $\delta f_{\text{bulk}}$  corrections for  $\delta f$ .

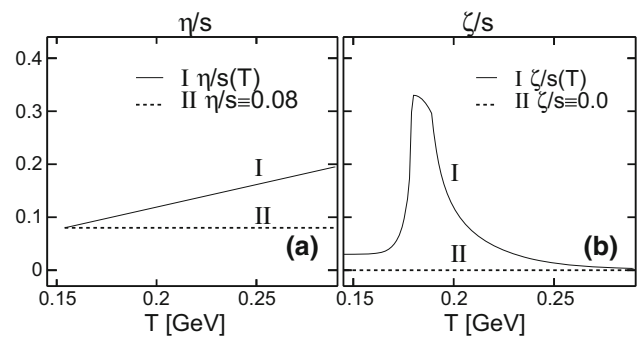


**Fig. 1** Two sets of specific shear viscosity  $\eta/s$  and specific bulk viscosity  $\zeta/s$  as a function of temperature, used in iEBE-VISHNU simulations with TRENTO initial condition (para-I) and AMPT initial condition (para-II)

effectively interpolates among different entropy deposition schemes, such as KLN, EKRT, WN, and so on [50, 51]. Following [51], we input a temperature-dependent specific shear viscosity  $\eta/s(T)$  and specific bulk viscosity  $\zeta/s(T)$  for the simulations with TRENTO initial condition. In Ref. [51], the specific shear viscosity  $\eta/s(T)$  above  $T_c$  was assumed to be a linear function with tunable minimum value and slope parameter. The specific bulk viscosity  $\zeta/s(T)$  was taken a peak form with two functions falls off exponentially at each side, together with a tunable overall normalization factor. Using Bayesian statistics, the free parameters of TRENTO the initial time  $\tau_0$ , switching temperature  $T_{sw}$ , and the parameterized  $\eta/s(T)$  and  $\zeta/s(T)$  in iEBE-VISHNU simulations, are simultaneously tuned through the massive data fitting of final multiplicity, mean  $p_T$  and integrated flow harmonics  $v_n$  in 2.76 A TeV Pb + Pb collisions. Such massive data evaluation prefers  $\tau_0 = 0.6$  fm/c,  $T_{sw} = 148$  MeV, together with the extracted  $\eta/s(T)$  and  $\zeta/s(T)$  curves shown in Fig. 1 (denoted as para-I). Other well calibrated parameters for TRENTO initial condition can be found in Table IV in [51].

In this paper, we study and predict various flow observables in both 2.76 and 5.02 A TeV Pb + Pb collisions. As shown in Fig. 2, the final multiplicities only increase by  $\sim 30\%$  after the collision energy is raised from 2.76 to 5.02 A TeV, which corresponds to  $\sim 10\%$  increase of the initial temperature. We thus use the same  $\eta/s(T)$  and  $\zeta/s(T)$  parametrization as well as other related parameter sets extracted in [51], except for re-tuning the normalization factor  $s_0$  in Eq. (4) to fit the final multiplicities of all charged hadrons in 5.02 A TeV Pb + Pb collisions.<sup>2</sup> We found that such parameter set-ups could equally well describe the measured flow harmonics of all charged hadrons in both 2.76 and 5.02 A TeV Pb + Pb collisions (see Sect. 4 for details).

<sup>2</sup> The centralities here and the ones for the following calculations in Sect. 4 are all cut by the distributions of all charged hadrons with  $|\eta| < 0.5$ .

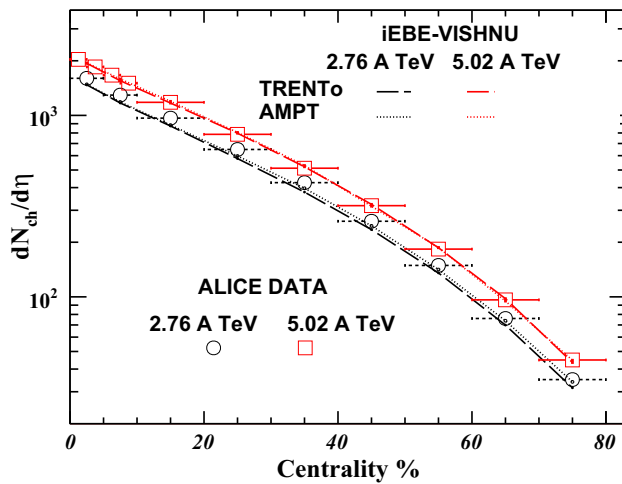


**Fig. 2** The centrality dependence of the charged-hadron multiplicity density  $dN_{ch}/d\eta$  ( $|\eta| < 0.5$ ) in Pb + Pb collisions at 2.76 and 5.02 A TeV, calculated from iEBE-VISHNU with TRENTo and AMPT initial conditions. The experimental data are taken from [71,72], respectively

The AMPT initial condition [26,68–70] constructs the initial energy density profiles through the energy decompositions of individual partons via a Gaussian smearing:

$$\epsilon = K \sum_i \frac{E_i^*}{2\pi\sigma^2\tau_0\Delta\eta_s} \exp\left(-\frac{(x-x_i)^2 + (y-y_i)^2}{2\sigma^2}\right), \quad (5)$$

where  $\sigma$  is the Gaussian smearing factor,  $E_i^*$  is the Lorentz invariant energy of the produced partons and  $K$  is an additional normalization factor. For simplicity, the initial flow is neglected as in Ref. [26,68,69] and the total produced partons from AMPT are truncated within  $|\eta| < 1$  to construct the initial energy density profiles in the transverse plane according to Eq. (5).

Following [26], we input a constant QGP specific shear viscosity and zero specific bulk viscosity, and set the parameters for the pre-equilibrium AMPT evolution: Lund string fragmentation  $a = 2.2$  and  $b = 0.5$ , strong coupling constant  $\alpha = 0.4714$  and the screening mass  $\mu = 3.226 \text{ fm}^{-1}$ . Considering that, from 2.76 to 5.02 A TeV Pb + Pb collisions, the final multiplicities only increase by  $\sim 30\%$ , we use the same hydrodynamic starting time  $\tau_0 = 0.6 \text{ fm}/c$ , transport coefficients  $\eta/s = 0.08$ ,  $\zeta/s = 0$  (denoted as para-II in Fig. 1) and Gaussian smearing factor  $\sigma = 0.6$ , and switching temperature  $T_{sw} = 148 \text{ MeV}$ , but we only tune the normalization factor  $K$  of the initial condition to fit the final multiplicities of all charged hadrons in 2.76 and 5.02 A TeV Pb + Pb collisions. We found such parameter set-ups can nicely fit the multiplicity,  $p_T$ -spectra and integrated flow harmonics  $v_n$  of all charged hadrons at these two collision energies (please

also refer to Sect. 4). The details of parameter tuning can be found in our earlier paper [26].

### 3 Flow observables

In this section, we briefly introduce the calculations of various flow observables that will be shown in the next section, which include flow harmonics  $v_n$ , event-by-event  $v_n$  distributions, event-plane correlations, the symmetric cumulants, non-linear response coefficients, and the  $p_T$ -dependent factorization ratios.

#### 3.1 Flow harmonics and the Q-cumulant method

The flow harmonics measure the anisotropy of momentum distributions of final produced hadrons, which can be obtained from a Fourier expansion of the event-averaged azimuthal particle distributions [73]:

$$\begin{aligned} \frac{dN}{d\varphi} &= \frac{1}{2\pi} \sum_{-\infty}^{\infty} V_n e^{-in\varphi} \\ &= \frac{1}{2\pi} \left( 1 + 2 \sum_{n=1}^{\infty} v_n e^{-in(\varphi - \Psi_n)} \right), \end{aligned} \quad (6)$$

where  $V_n$  is the  $n$ th order flow vector, defined as  $V_n = v_n e^{in\Psi_n}$ ,  $v_n = \langle \cos n(\varphi - \Psi_n) \rangle$  is the  $n$ th flow harmonics and  $\Psi_n$  is the corresponding event-plane angle.

The generally used Q-cumulant method [74] measures the flow harmonics  $v_n$  from 2- and multi-particle correlations without the knowledge of the event plane. The  $Q_n$ -vector is defined by

$$Q_n = \sum_{i=1}^M e^{in\varphi_i}, \quad (7)$$

where  $M$  is the multiplicity in a single event and  $\varphi_i$  is the azimuthal angle of the emitted particle  $i$ . With this  $Q_n$ -vector, the 2- and 4-particle azimuthal correlations in a single event can be calculated as [74]:

$$\begin{aligned} \langle 2 \rangle_{n,-n} &= \frac{|Q_n|^2 - M}{M(M-1)}, \\ \langle 4 \rangle_{n,n,-n,-n} &= \frac{|Q_n|^4 + |Q_{2n}|^2 - 2 \cdot \text{Re}[Q_{2n} Q_n^* Q_n^*]}{M(M-1)(M-2)(M-3)} \\ &\quad - 2 \frac{2(M-2) \cdot |Q_n|^2 - M(M-3)}{M(M-1)(M-2)(M-3)}, \end{aligned} \quad (8)$$

Here, we have used the general notation of the single-event  $k$ -particle correlators  $\langle k \rangle_{n_1, n_2, \dots, n_k} \equiv \langle \cos(n_1\varphi_1 + n_2\varphi_2 + \dots + n_k\varphi_k) \rangle$  ( $n_1 \geq n_2 \geq \dots \geq n_k$ ) and  $\langle \dots \rangle$  means an average over all the particles in a single event. After averaging

over the whole events within the selected centrality bin, the obtained 2- and 4-particle cumulants are:

$$c_n\{2\} = \langle\langle 2 \rangle\rangle_{n,-n},$$

$$c_n\{4\} = \langle\langle 4 \rangle\rangle_{n,n,-n,-n} - 2 \cdot \langle\langle 2 \rangle\rangle_{n,-n}^2. \tag{9}$$

Then the 2- and 4-particle integrated flow harmonics can be calculated as [74]:

$$v_n\{2\} = \sqrt{c_n\{2\}}, \quad v_n\{4\} = \sqrt[4]{-c_n\{4\}}. \tag{10}$$

In general, the non-flow effects from jets, resonance decays, etc. could be largely suppressed by the 4-particle correlations of the flow harmonics  $v_n\{4\}$ . However, they still significantly influence  $v_n\{2\}$  obtained from the 2-particle correlations. To suppress such non-flow effects, one divides the whole event into two sub-events with a certain pseudorapidity gap  $|\Delta\eta|$ , and then one calculates the modified 2-particle azimuthal correlations:

$$\langle 2 \rangle_{n,-n}^{|\Delta\eta|} = \frac{Q_n^A Q_n^{B*}}{M_A M_B}, \tag{11}$$

where  $Q_n^{A(B)}$  and  $M_{A(B)}$  are the  $Q_n$ -vectors and multiplicities of sub-event A(B). The Q-cumulant and flow harmonics from 2-particle correlations with a  $|\Delta\eta|$  gap become

$$c_n\{2, |\Delta\eta|\} = \langle\langle 2 \rangle\rangle_{n,-n}^{|\Delta\eta|}, \quad v_n\{2, |\Delta\eta|\} = \sqrt{c_n\{2, |\Delta\eta|\}}. \tag{12}$$

One could also define a single-event correlator averaged over the Particles Of Interests (POIs). Such POIs can be some specific identified hadrons or hadrons within some transverse momentum ranges and so on, depending on the physics of interest. With the correlators of POIs, one can further calculate the (differential) flow harmonics of all charged hadrons or identified hadrons in a similar way as described above. Again the non-flow effects can be suppressed by a pseudorapidity gap  $|\Delta\eta|$ . Due to the limited space, we will not further outline the lengthy formulas, but refer to [74, 75] for details.

Note that the scalar-product (SP) method also belongs to the framework of two-particle correlations, but uses different event average weights when compared with the standard Q-cumulant method [74]. We found that, for the iEBE-VISHNU hybrid model simulations with non-flows mainly contributed from resonance decays, the Q-cumulant method and the scalar-product method generate almost identical flow harmonics from semi-central to semi-peripheral collisions [26, 76]

### 3.2 Distributions of event-by-event flow harmonics

The event-by-event  $v_n$  distributions reflect the event-by-event fluctuations of the initial states of relativistic heavy-ion collisions, which are not significantly influenced by the hydro-

dynamic evolution and can provide strong constraints for the initial condition models [27, 28, 77].

In general, one first calculates the per-particle flows from an expansion of the particle distributions in azimuthal angle  $\phi$  and then obtains the event-by-event distributions of flow harmonics in a selected centrality bin. However, finite multiplicities and non-flow effects can make the distributions of observed per-particle flow deviate from the true distributions. To suppress such effects, one implements the standard Bayesian unfolding procedure [28, 78] to obtain the true  $v_n$  distributions. Due to the limited spaces, we do not outline the details to calculate the  $v_n$  distributions and the related Bayesian unfolding procedure, but refer to [28, 78] for details.

For a selected centrality bin, the averaged flow harmonics  $\langle v_n \rangle$  from model calculations and experimental measurements are not exactly the same, but there exist some differences. To get rid of such influences and focus on the shape of the  $v_n$  distributions, one defines the scaled event-by-event  $v_n$  distributions  $P(v_n / \langle v_n \rangle)$ , which are generally used to evaluate the related model calculations with certain initial conditions [27, 28].

### 3.3 Event-plane correlations

The event-plane correlations evaluate the correlations of various flow angle combinations, which shed lights on the initial state fluctuations and the non-linear response of the evolving system [31–35]. Following [31, 33], we implement the scalar-product method to calculate the event-plane correlations. The two and three event-plane correlations are defined by

$$\begin{aligned} & \cos [c_1 n_1 \Psi_{n_1} - c_2 n_2 \Psi_{n_2}] \\ &= \frac{\langle \tilde{Q}_{n_1 A}^{c_1} \tilde{Q}_{n_2 B}^{c_2*} \rangle}{\sqrt{\langle \tilde{Q}_{n_1 A}^{c_1} \tilde{Q}_{n_1 B}^{c_1*} \rangle} \sqrt{\langle \tilde{Q}_{n_2 A}^{c_2} \tilde{Q}_{n_2 B}^{c_2*} \rangle}} \\ & \cos [c_1 n_1 \Psi_{n_1} + c_2 n_2 \Psi_{n_2} - c_3 n_3 \Psi_{n_3}] \\ &= \frac{\langle \tilde{Q}_{n_1 A}^{c_1} \tilde{Q}_{n_2 A}^{c_2} \tilde{Q}_{n_3 B}^{c_3*} \rangle}{\sqrt{\langle \tilde{Q}_{n_1 A}^{c_1} \tilde{Q}_{n_1 B}^{c_1*} \rangle} \sqrt{\langle \tilde{Q}_{n_2 A}^{c_2} \tilde{Q}_{n_2 B}^{c_2*} \rangle} \sqrt{\langle \tilde{Q}_{n_3 A}^{c_3} \tilde{Q}_{n_3 B}^{c_3*} \rangle}}, \end{aligned} \tag{13}$$

Here, the subscripts “A” and “B” denote the two different sub-events, which are separated by a  $|\Delta\eta|$  gap. The reduced flow vector  $\tilde{Q}_n$  is defined by

$$\tilde{Q}_n \equiv \frac{1}{N} \sum_j e^{in\varphi_j}, \tag{14}$$

where  $N$  is the number of particles in a sub-event, and  $\varphi_j$  is azimuthal angles of particle  $i$ . Note that, for a specific two or three event-plane correlator, the azimuthal symmetry

requires that  $c_1n_1 - c_2n_2 = 0$  or  $c_1n_1 + c_2n_2 - c_3n_3 = 0$  [31,33].

### 3.4 The symmetric cumulant

The symmetric cumulant  $SC(m, n)$  measures the correlations between different flow harmonics, which is defined by [35, 37, 79]

$$\begin{aligned} SC^v(m, n) &= \langle\langle \cos(m\varphi_1 + n\varphi_2 - m\varphi_3 - n\varphi_4) \rangle\rangle_c \\ &= \langle\langle 4 \rangle\rangle_{n,m,-n,-m} - \langle\langle 2 \rangle\rangle_{n,-n} \cdot \langle\langle 2 \rangle\rangle_{m,-m} \\ &= \langle v_m^2 v_n^2 \rangle - \langle v_m^2 \rangle \langle v_n^2 \rangle. \end{aligned} \tag{15}$$

Here the symmetric cumulant is only defined with  $m \neq n$  for two positive integers  $m$  and  $n$ . The single-event 4-particle and 2-particle correlations  $\langle 4 \rangle_{n,m,-n,-m}$ ,  $\langle 2 \rangle_{n,-n}$  and  $\langle 2 \rangle_{m,-m}$  can be expressed in terms of the Q-vectors (please refer to [35, 37] for details), and  $\langle\langle \dots \rangle\rangle$  denotes an average over all the events.

To evaluate the relative strength of the correlations between different flow harmonics, one defines the normalized symmetric cumulants:

$$NSC^v(m, n) = \frac{SC^v(m, n)}{\langle v_m^2 \rangle \langle v_n^2 \rangle}, \tag{16}$$

where  $\langle v_m^2 \rangle$  and  $\langle v_n^2 \rangle$  can be calculated by the 2-particle cumulants in Eq.(10). For details, see [37,40].

### 3.5 Non-linear response coefficients

The non-linear evolution of the QGP fireball leads to the mode couplings between different flow harmonics, which could be evaluated by the non-linear response coefficients [35,80,81]. Except for the second and third order anisotropic flows which are linearly proportional to second and third order eccentricities of the initial state, the higher-order anisotropic flow vectors contain contributions of both linear and nonlinear parts, which can be decomposed as [35,80,81]

$$\begin{aligned} V_4 &= V_{4L} + \chi_{422} V_2^2, \quad V_5 = V_{5L} + \chi_{523} V_2 V_3, \\ V_6 &= V_{6L} + \chi_{624} V_2 V_{4L} + \chi_{633} V_3^2 + \chi_{6222} V_2^3, \\ V_7 &= V_{7L} + \chi_{725} V_2 V_{5L} + \chi_{734} V_3 V_{4L} + \chi_{7223} V_2^2 V_3. \end{aligned} \tag{17}$$

Here, the non-linear terms directly involve the contributions from lower order flow anisotropies and the corresponding coefficients  $\chi_{mnl}$  and  $\chi_{mnlk}$  are called the non-linear response coefficients (mode-coupling coefficients). Following [81], we implement the scalar-product method to calculate the mode-coupling coefficients, which are expressed as

$$\chi_{422} = \frac{\langle \tilde{Q}_{4A} \tilde{Q}_{2B}^* \tilde{Q}_{2B}^* \rangle}{\langle \tilde{Q}_{2A} \tilde{Q}_{2A} \tilde{Q}_{2B}^* \tilde{Q}_{2B}^* \rangle},$$

$$\begin{aligned} \chi_{523} &= \frac{\langle \tilde{Q}_{5A} \tilde{Q}_{2B}^* \tilde{Q}_{3B}^* \rangle}{\langle \tilde{Q}_{2A} \tilde{Q}_{3A} \tilde{Q}_{2B}^* \tilde{Q}_{3B}^* \rangle}, \\ \chi_{624} &= \frac{\langle \tilde{Q}_{6A} \tilde{Q}_{2B}^* \tilde{Q}_{4B}^* \rangle \langle \tilde{Q}_{2A}^2 \tilde{Q}_{2B}^{*2} \rangle - \langle \tilde{Q}_{6A} \tilde{Q}_{2B}^{*3} \rangle \langle \tilde{Q}_{4A} \tilde{Q}_{2B}^{*2} \rangle}{(\langle \tilde{Q}_{4A} \tilde{Q}_{4B}^* \rangle \langle \tilde{Q}_{2A}^2 \tilde{Q}_{2B}^{*2} \rangle - \langle \tilde{Q}_{4A} \tilde{Q}_{2B}^{*2} \rangle^2) \langle \tilde{Q}_{2A} \tilde{Q}_{2B}^* \rangle}, \\ \chi_{633} &= \frac{\langle \tilde{Q}_{6A} \tilde{Q}_{3B}^* \rangle}{\langle \tilde{Q}_{3A}^2 \tilde{Q}_{3B}^{*2} \rangle}, \quad \chi_{6222} = \frac{\langle \tilde{Q}_{6A} \tilde{Q}_{2B}^{*3} \rangle}{\langle \tilde{Q}_{2A} \tilde{Q}_{2B}^* \rangle^3}, \\ \chi_{734} &= \frac{\langle \tilde{Q}_{7A} \tilde{Q}_{3B}^* \tilde{Q}_{4B}^* \rangle \langle \tilde{Q}_{2A} \tilde{Q}_{2B}^{*2} \rangle - \langle \tilde{Q}_{7A} \tilde{Q}_{2B}^{*2} \tilde{Q}_{3B}^* \rangle \langle \tilde{Q}_{4A} \tilde{Q}_{2B}^{*2} \rangle}{(\langle \tilde{Q}_{4A} \tilde{Q}_{4B}^* \rangle \langle \tilde{Q}_{2A} \tilde{Q}_{2B}^{*2} \rangle - \langle \tilde{Q}_{4A} \tilde{Q}_{2B}^{*2} \rangle^2) \langle \tilde{Q}_{3A} \tilde{Q}_{3B}^* \rangle}, \\ \chi_{725} &= \frac{\langle \tilde{Q}_{7A} \tilde{Q}_{2B}^* \tilde{Q}_{5B}^* \rangle \langle \tilde{Q}_{2A} \tilde{Q}_{2B}^* \tilde{Q}_{3A} \tilde{Q}_{3B}^* \rangle - \langle \tilde{Q}_{7A} \tilde{Q}_{2B}^{*2} \tilde{Q}_{3B}^* \rangle \langle \tilde{Q}_{5A} \tilde{Q}_{2B}^* \tilde{Q}_{3B}^* \rangle}{(\langle \tilde{Q}_{5A} \tilde{Q}_{5B}^* \rangle \langle \tilde{Q}_{2A} \tilde{Q}_{2B}^* \tilde{Q}_{3A} \tilde{Q}_{3B}^* \rangle - \langle \tilde{Q}_{5A} \tilde{Q}_{2B}^* \tilde{Q}_{3B}^* \rangle^2) \langle \tilde{Q}_{2A} \tilde{Q}_{2B}^* \rangle}, \\ \chi_{7223} &= \frac{\langle \tilde{Q}_{7A} \tilde{Q}_{2B}^{*2} \tilde{Q}_{3B}^* \rangle}{\langle \tilde{Q}_{2A}^2 \tilde{Q}_{2B}^{*2} \tilde{Q}_{3A} \tilde{Q}_{3B}^* \rangle}. \end{aligned} \tag{18}$$

Here, the whole event is divided into two sub-events, A and B, with a  $|\Delta\eta|$  gap separation to suppress the non-flow effects. The reduced flow vectors  $\tilde{Q}_{nA}$  and  $\tilde{Q}_{nB}$  are defined by Eq. (14), and  $\langle \dots \rangle$  means averaging over the whole events, and then taking the real parts.

### 3.6 $p_T$ -dependent factorization ratio

The produced hadrons at different transverse momentum  $p_T$  do not share a common flow angle, which leads to the break-up of the flow harmonics factorizations. To evaluate the strength of such break-ups, one defines the  $p_T$ -dependent factorization ratio [42,44]:

$$r_n(p_T^a, p_T^b) \equiv \frac{V_{n\Delta}(p_T^a, p_T^b)}{\sqrt{V_{n\Delta}(p_T^a, p_T^a) V_{n\Delta}(p_T^b, p_T^b)}}, \tag{19}$$

Here,  $V_{n\Delta}$  is the average value of  $\cos(n\Delta\phi)$  for all particles pairs within a momentum bin range, together with a  $|\Delta\eta|$  gap to reduce the non-flow effects. It can be calculated as [44]:

$$V_{n\Delta} \equiv \langle\langle \cos(n\Delta\phi) \rangle\rangle = \langle \tilde{Q}_n^{a(b)} \tilde{Q}_n^{a(b)*} \rangle, \tag{20}$$

where  $\langle\langle \dots \rangle\rangle$  denotes averaging over all particle pairs in a single event and then taking an average over all events.  $\tilde{Q}_n^{a(b)}$  is the reduced flow vector of POIs calculated within a specific  $p_T^{a(b)}$  bin and rapidity range:  $\tilde{Q}_n^{a(b)} \equiv \frac{1}{N} \sum_j e^{in\varphi_j}$ . The related average  $\langle \dots \rangle$  means averaging over the whole events and then taking the real part.

## 4 Results and discussions

In this paper, we implement iEBE-VISHNU hybrid model with TRENTO and AMPT initial conditions to study and predict various flow observables in 2.76 and 5.02 A TeV Pb + Pb collisions. In practice, we first fix the free inputs in iEBE-VISHNU (e.g. transport coefficients and the hydrodynamic starting time  $\tau_0$ ) as well as the free parameters in TRENTO and AMPT from fitting the multiplicity of total charged hadrons,  $p_T$  spectra of identified hadrons, and the

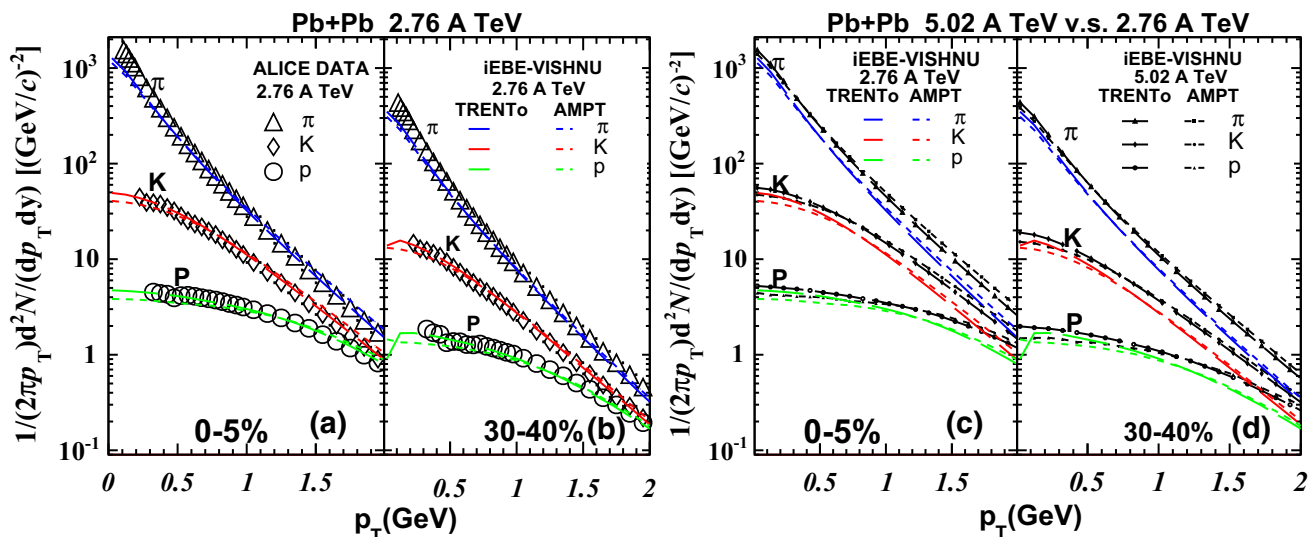


**Fig. 3**  $p_T$  spectra of pions, kaons, and protons in 0–5 and 30–40% Pb + Pb collisions at 2.76 and 5.02 A TeV, calculated from iEBE-VISHNU with TRENTo and AMPT initial conditions. The experimental data at 2.76 A TeV are taken from the ALICE paper [82]

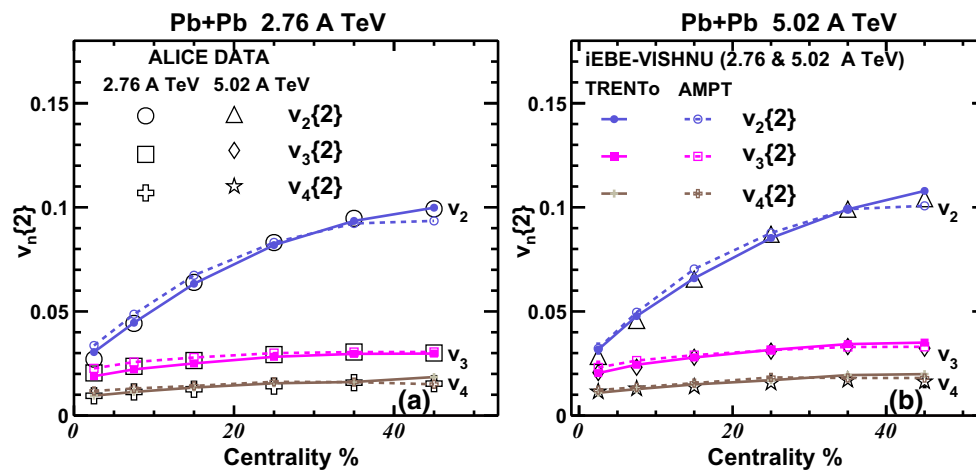
integrated flow harmonics  $v_n$  of total charged hadrons, and then we make predictions for other flow observables, including the differential flow harmonics  $v_n(p_T)$  of identified hadrons, the event-by-event  $v_n$  distributions, the event-plane correlations, the symmetric cumulants, non-linear response coefficients and the  $p_T$ -dependent factorization ratios.

Figure 3 shows the  $p_T$  spectra of pions, kaons, and protons in 0–5 and 30–40% Pb + Pb collisions at 2.76 and 5.02 A TeV. The left two panels compare iEBE-VISHNU calculations with the ALICE data [82] at 2.76 A TeV. For both TRENTo and AMPT initial conditions, iEBE-VISHNU nicely fits the data for these two selected centrality bins, which indicates that hybrid model simulations generate proper amounts of radial flow. Note that the slope of the  $p_T$  spectra is sensitive to the initial time  $\tau_0$  and the switching temperature  $T_{\text{switch}}$ . The massive data evaluations from early iEBE-VISHNU simulations with TRENTo initial conditions prefer  $T_{\text{switch}} = 148$  MeV and  $\tau_0 = 0.6$  fm/c in 2.76 A TeV Pb + Pb collisions [51]. For simulations with the AMPT initial conditions, we continue to use the same values of  $T_{\text{switch}}$  and  $\tau_0$ . This leads to slightly softer  $p_T$  spectra for protons and slightly harder  $p_T$  spectra for pions compared with the results obtained with the TRENTo initial conditions, but still makes an overall good fit of the measured data below 2 GeV.

Figure 3c and d show the VISHNU predictions for the  $p_T$ -spectra of pions, kaons and protons in 5.02 A TeV Pb + Pb collisions. As introduced in Sect. 2, we use almost the same parameter sets as the ones at 2.76 A TeV, except for tuning the normalization factors of the initial entropy/energy densities to achieve a nice fit of the final multiplicities of all charged hadrons in 5.02 A TeV Pb + Pb collisions. Panels (c)

and (d) show that the  $p_T$ -spectra in 5.02 A TeV are higher and flatter than the ones in 2.76 A TeV, which illustrates that stronger radial flow has been developed in the systems with larger final multiplicities at higher collision energy.

Figure 4 shows the integrated flow harmonics  $v_n$  ( $n = 2-4$ ) of all charged hadrons in 2.76 and 5.02 A TeV Pb + Pb collisions. Following [20,52], we calculate the flow harmonics  $v_n$  using the 2-particle cumulant method within  $0.2 < p_T < 5.0$  GeV and  $|\eta| < 0.8$ , together with a pseudo rapidity gap  $|\Delta\eta| > 1.0$ . For both TRENTo and AMPT initial conditions, the transport coefficients and other related parameters in iEBE-VISHNU have been fine tuned to fit the flow harmonics  $v_n$  in 2.76 A TeV Pb + Pb collisions (please refer to Sect. 2 for details). We found, with the extracted  $\eta/s(T)$  and  $\zeta/s(T)$  (para-I in Fig. 1) for TRENTo initial condition and  $\eta/s = 0.08$  and  $\zeta/s = 0$  (para-II in Fig. 1) for AMPT initial condition, iEBE-VISHNU can nicely describe the centrality-dependent flow harmonics  $v_n$  in both 2.76 and 5.02 A TeV Pb + Pb collisions. The comparison runs in [55] also showed that, with the same sets of transport coefficients, MUSIC+IP-Glasma simulations can nicely fit the  $v_n$  data at these two collision energies. In contrast, the early calculations of the flow harmonics in 200 A GeV Au+Au collisions and 2.76 A TeV Pb + Pb collisions indicated that the average QGP shear viscosity is slightly larger at the LHC than at RHIC, when the final multiplicities increase by about a factor of 2 [14,24]. In fact, the final multiplicities between 2.76 and 5.02 A TeV Pb + Pb collisions only differ by  $\sim 30\%$ , which corresponds to  $\sim 10\%$  change of the initial temperature. We thus do not fine-tune the transport coefficients for each collision energy, but we use the same parameter sets. We find that such choice of parameters can simultaneously



**Fig. 4** Integrated flow  $v_n$  ( $n=2-4$ ) of all charged hadrons in Pb + Pb collisions at 2.76 A TeV (left panel) and 5.02 A TeV (right panel), calculated from iEBE-VISHNU with TRENTo and AMPT initial conditions. The experimental data are taken from [20,52], respectively

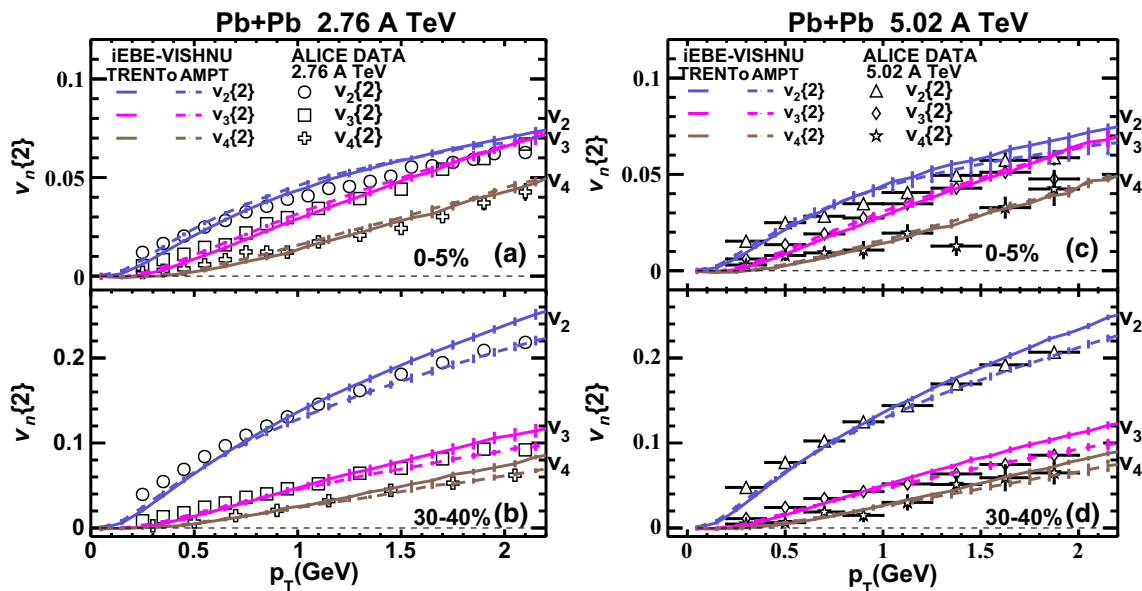


**Fig. 5** The differential flow harmonics  $v_n(p_T)$  ( $n=2-4$ ) of all charged hadrons in 0–5 and 30–40% Pb + Pb collisions at 2.76 A TeV (left panels) and 5.02 A TeV (right panels), calculated from iEBE-VISHNU with TRENTo and AMPT initial conditions. The experimental data are taken from [20,52], respectively

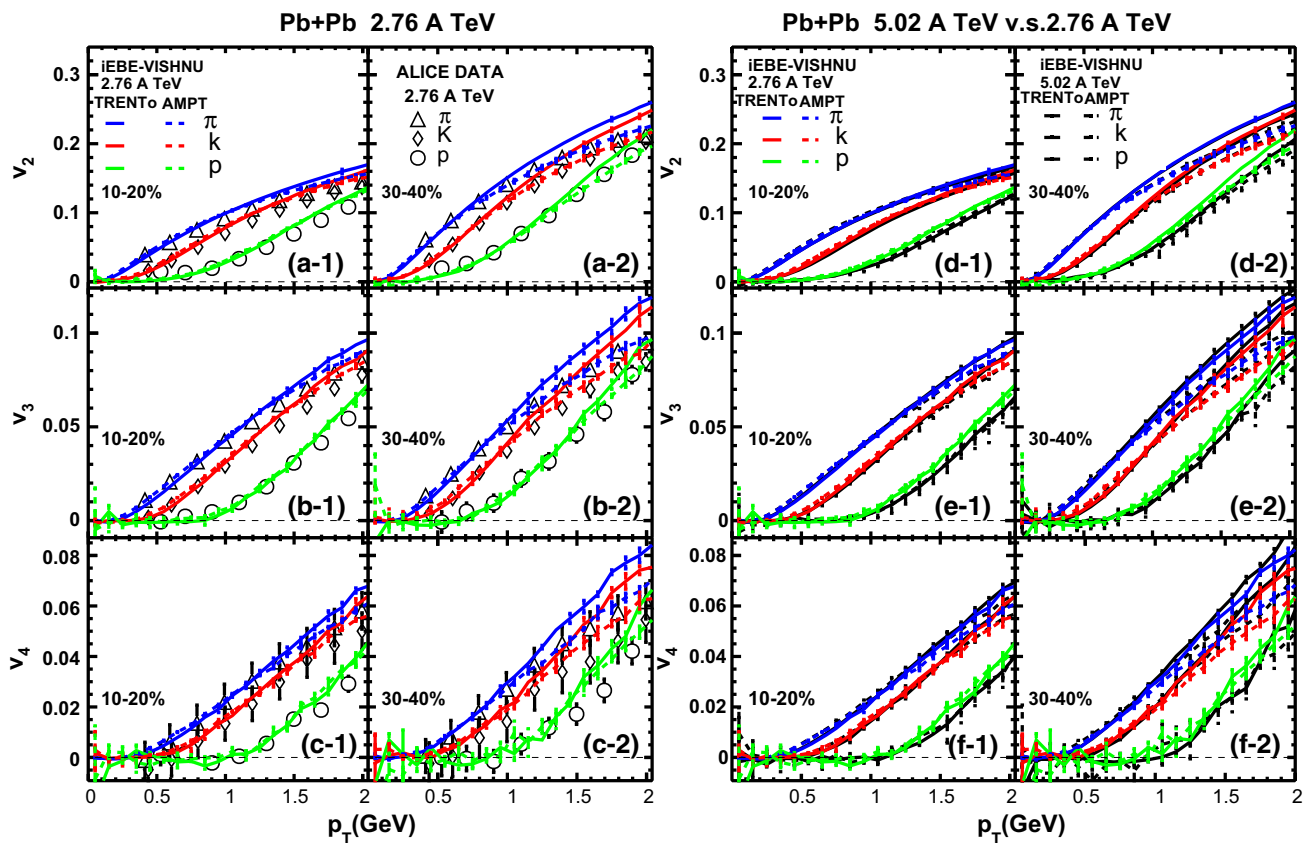
fit the individual flow harmonics in both 2.76 and 5.02 A TeV Pb + Pb collisions.

Figure 5 shows the differential flow harmonics  $v_n(p_T)$  ( $n=2-4$ ) of all charged hadron in 0–5 and 30–40% Pb + Pb collisions at 2.76 and 5.02 A TeV, calculated by iEBE-VISHNU and measured by ALICE using the 2-particle cumulant method within  $|\eta| < 0.8$ .<sup>3</sup> For TRENTo

<sup>3</sup> Instead of imposing a pseudorapidity cut  $|\Delta\eta| > 1.0$  as [20,52], we calculate the 2-particle cumulants using two sub-events with  $|\Delta\eta| > 0$  in order to reduce the error bars of the limited iEBE-VISHNU runs. The non-flow effects in iEBE-VISHNU are dominated by resonance decays. The past simulations [26,76] have shown that the  $v_n(p_T)$  curves with  $|\Delta\eta| > 0$  and  $|\Delta\eta| > 0.8$  cuts almost overlap with each other.

initial conditions, iEBE-VISHNU roughly fits the ALICE data in these two collision energies, but with slightly larger slopes. This leads to over-predictions of the  $v_n(p_T)$  data above 1 GeV, especially for the 30–40% centrality. In fact, the parameter sets used in our calculations were obtained from the massive data fitting of the particle yields the mean  $p_T$  and integrated flow harmonics in 2.76 A TeV Pb + Pb collisions [51]. Considering the relatively larger error bars, the differential flow harmonics  $v_n(p_T)$  were not included in the early massive data evaluations. This partially explains why the current iEBE-VISHNU simulations with TRENTo initial conditions do not perfectly describe the  $v_n(p_T)$  data. Note that the MUSIC + IP-Glasma simulations [55] also





**Fig. 6** The differential flow harmonics  $v_n(p_T)$  ( $n = 2-4$ ) of pions, kaons and protons in 10–20 and 30–40% Pb + Pb collisions at 2.76 A TeV (left panels) and 5.02 A TeV (right panels), calculated from

iEBE-VISHNU with TRENTo and AMPT initial conditions. The experimental data at 2.76 A TeV are taken from [83]

over-predicted the slope of the  $v_n(p_T)$  curves and did not fit the  $v_n(p_T)$  data very nicely in both 2.76 and 5.02 A TeV Pb + Pb collisions. Compared with these two simulations, iEBE-VISHNU with AMPT initial condition gives a better description of the data, especially for 30–40% centrality. We have also noticed that  $v_n(p_T)$  data below 0.5 GeV are all slightly under-predicted for these simulations with different initial conditions. In [83], it was pointed out that the  $v_n(p_T)$  data at lower  $p_T$  region may be contaminated by residual non-flow effects, which have not been fully removed.

Figure 6 shows the differential flow harmonics  $v_n(p_T)$  ( $n = 2-4$ ) of identified hadrons in 10–20 and 30–40% Pb + Pb collisions at 2.76 and 5.02 A TeV. Following [83], we calculate  $v_n(p_T)$  using the scalar-product method with particle of interest (POIs) and reference particles (RPs) selected from two sub-events within  $-0.8 < \eta < 0$  and  $0 < \eta < 0.8$ . Note that the residue non-flow effects have been subtracted from the ALICE data at 2.76 A TeV using the corrections from p-p collisions [83]. This is not necessary for our iEBE-VISHNU calculations since the related non-flow effects are mainly from resonance decays. The left panels (a)–(c) compare our model calculations with the data in 2.76 A TeV Pb + Pb collisions. For TRENTo initial condition, iEBE-VISHNU

can roughly describe the  $v_n(p_T)$  of pions, kaons and protons at 10–20% centrality, but over-predicts the  $v_n(p_T)$  above 1 GeV at 30–40% centrality. For the AMPT initial condition, iEBE-VISHNU gives an overall quantitative description of the ALICE data for these two selected centrality bins. The situation is similar to the case in Fig. 5, since  $v_n(p_T)$  of the identified hadrons reflect both the total momentum anisotropies and their distributions among various hadron species.

In the right panels (d–f), we predict  $v_n(p_T)$  ( $n = 2-4$ ) of pions, kaons and protons in 5.02 A TeV Pb + Pb collisions, together with a comparison to the iEBE-VISHNU results in 2.76 A TeV Pb + Pb collisions. For both TRENTo and AMPT initial conditions, the differences between these two collision energies are pretty small, which also show similar  $v_n$  mass-orderings. Note that the measured and calculated  $v_n(p_T)$  ( $n = 2-4$ ) of all charged hadrons also almost overlap between these two collision energies (please refer to Fig. 5 in this paper and Fig. 2 in [52]). The early comparison of the flow harmonics at RHIC and the LHC has shown that  $v_2(p_T)$  of all charged hadrons almost overlap, while the  $v_2$  mass splittings between pions and protons are enlarged with the increase of collision energy [84]. As shown in Fig. 6, the  $v_n$  mass splittings between pions and protons slightly increase

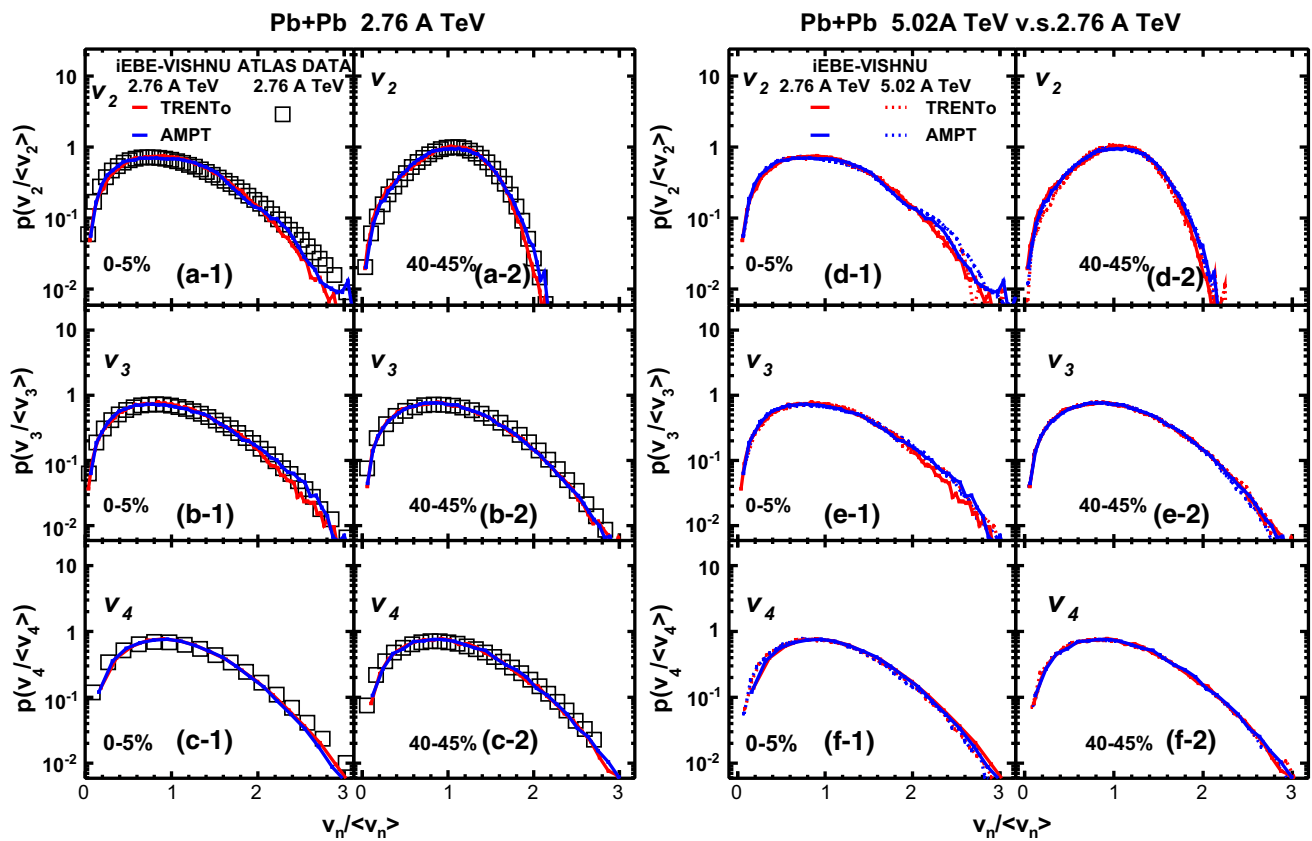


**Fig. 7** The scaled event-by-event  $v_n$  distributions in 0–5 and 40–45% Pb + Pb collisions at 2.76 and 5.02 A TeV, calculated from *iEBE-VISHNU* with TRENTo and AMPT initial conditions. The experimental data at 2.76 A TeV are taken from the ATLAS paper [28]

from 2.76 to 5.02 A TeV due to the slightly increased radial flow.

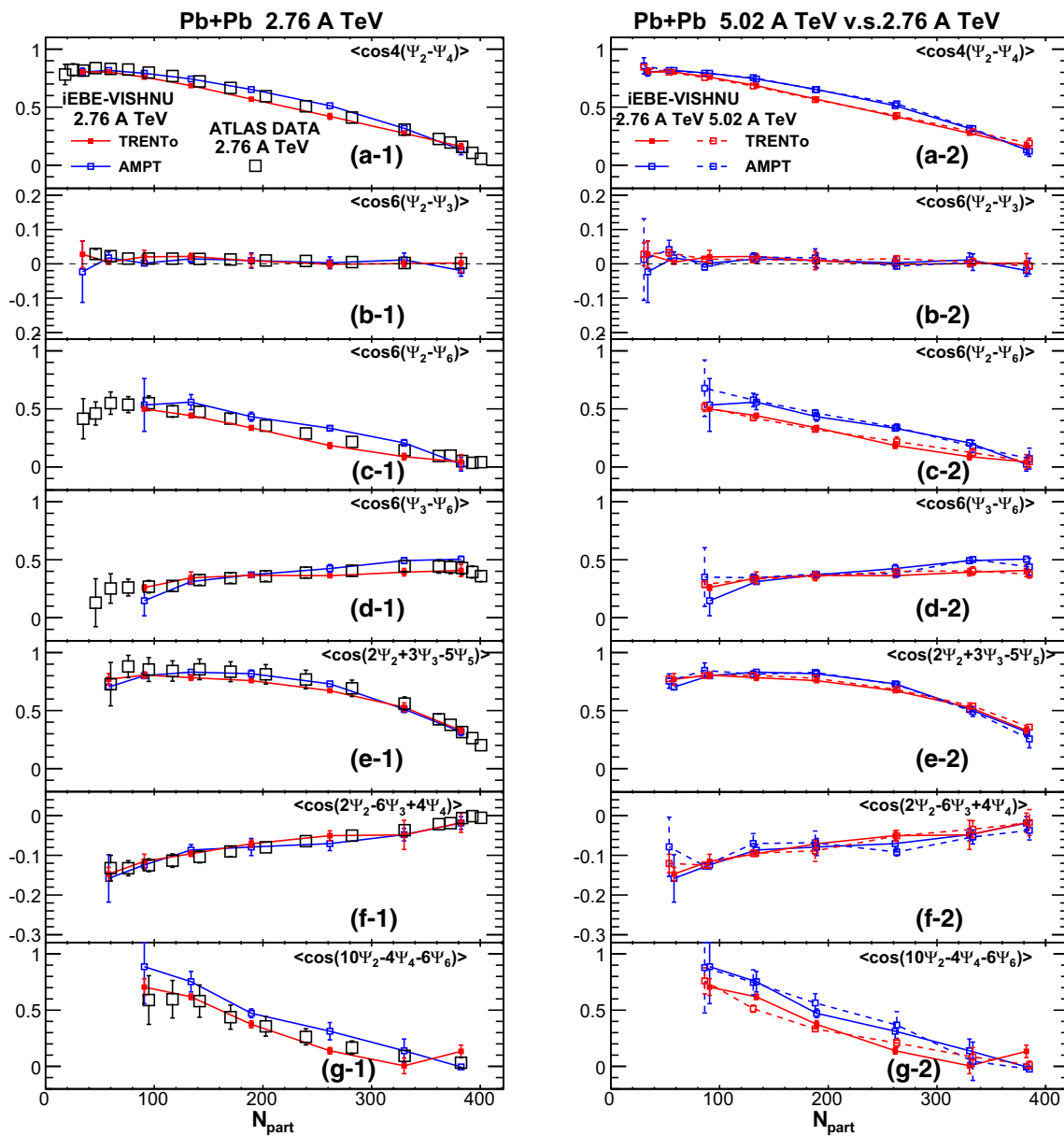
In Ref. [55], the differential flow harmonics  $v_2(p_T)$  of  $\Lambda$ ,  $\Xi$  and  $\phi$  have also been predicted, which showed certain mass-ordering patterns among these strange and multi-strange hadrons. While, other early research showed that the  $v_2$  mass-orderings between  $\Lambda$  and p are largely influenced by the pre-equilibrium flow [85] and the magnitude of the  $v_2^\phi$  is sensitive to the interaction between the  $\phi$  meson and the hadronic matter [25]. Considering these complexities and the requirement of much higher statistical runs for the model calculations, we do not further predict  $v_n(p_T)$  of these strange and multi-strange hadrons, but leave this to future study.

Figure 7 shows the scaled event-by-event  $v_n$  distributions ( $n = 2-4$ ) in 0–5 and 40–45% Pb + Pb collisions at 2.76 and 5.02 A TeV. Following [28], we first calculate the integrated  $v_2$  within transverse momentum  $p_T > 0.5$  GeV and pseudorapidity  $|\eta| < 2.5$ , using the single-particle method, and then perform the standard Bayesian unfolding procedure [28, 78] to obtain the “true”  $v_n$  distributions. The left panels (a)–(c) compare the measured and calculated scaled  $v_n$  distributions  $P(v_n/\langle v_n \rangle)$  in 2.76 A TeV Pb + Pb collisions. For both AMPT and TRENTo initial conditions,

*iEBE-VISHNU* nicely describes the measured  $P(v_n/\langle v_n \rangle)$  curves from ATLAS. As observed in [27], the scaled  $v_n$  distributions follow the scaled  $\varepsilon_n$  distributions, for  $n = 2$  and 3, due to the linear hydrodynamic response. For  $n = 4$ , the scaled  $\varepsilon_n$  distributions show small deviations from the experimental data in semi-central Pb + Pb collisions [27]. The non-linear hydrodynamic evolution couples the modes between  $n = 2$  and  $n = 4$ , leading to a nice description of the  $P(v_n/\langle v_n \rangle)$  data for  $n = 4$ .

The right panels (d–f) show *iEBE-VISHNU* predictions for the scaled  $v_n$  distributions in 0–5 and 40–45% Pb + Pb collisions at 5.02 A TeV, together with a comparison with the results at 2.76 A TeV. For both TRENTo and AMPT initial conditions, the  $P(v_n/\langle v_n \rangle)$  curves at these two collision energies overlap with each other. As discussed above, the scaled  $v_n$  distributions mostly follow the scaled  $\varepsilon_n$  distributions, which thus are insensitive to the collision energy.

Figure 8 shows the event-plane correlations as a function of participant number in Pb + Pb collisions at 2.76 and 5.02 A TeV. Following the ATLAS paper [31], we calculate the event-plane correlations using the scalar-product method with a pseudorapidity gap  $|\Delta\eta| > 1.0$  and within  $p_T > 0.5$  GeV and  $|\eta| < 2.5$ . The left panels show that, for



**Fig. 8** Event-plane correlations as a function of participant number in Pb + Pb collisions at 2.76 and 5.02 A TeV, calculated from iEBE-VISHNU with TRENTo and AMPT initial conditions. The data at 2.76 A TeV are taken from the ATLAS paper [31], and the  $N_{part}$  values are taken from [31, 72]

both TRENTo and AMPT initial conditions, iEBE-VISHNU can roughly reproduce the ATLAS data in 2.76 A TeV Pb + Pb collision.<sup>4</sup> More specifically, our model calculations nicely describe the decreasing trends of  $\langle \cos 4(\Psi_2 - \Psi_4) \rangle$ ,  $\langle \cos 6(\Psi_2 - \Psi_6) \rangle$ ,  $\langle \cos(2\Psi_2 + 3\Psi_3 - 5\Psi_5) \rangle$  and  $\langle \cos(10\Psi_2 - 4\Psi_4 - 6\Psi_6) \rangle$ , and the increasing trends of  $\langle \cos 6(\Psi_3 - \Psi_6) \rangle$  and  $\langle \cos(2\Psi_2 - 6\Psi_3 + 4\Psi_4) \rangle$  with the increase of the participant number, which also shows close to zero values for  $\langle \cos 6(\Psi_2 - \Psi_3) \rangle$ , as measured in experiments. In Ref. [32],

<sup>4</sup> For the limited space, we do not plot all 14 event-plane correlations as measured in experiments, but only show seven representative correlations.

it was found that the non-linear mode couplings and the related event-plane rotations during the hydrodynamic evolution are essential for a qualitative description of various centrality-dependent correlations, which even flip the signs of some correlators between initial and final states. Their calculations also showed that event-plane correlations are sensitive to both initial conditions and the QGP shear viscosity [32]. However, the early VISH2+1 calculations, with either MC-Glauber or MC-KLN initial conditions, failed to quantitatively describe all the measured event-plane correlation data. In fact, both of these two initial conditions also have difficulties to fit all the flow harmonics  $v_n$  as well

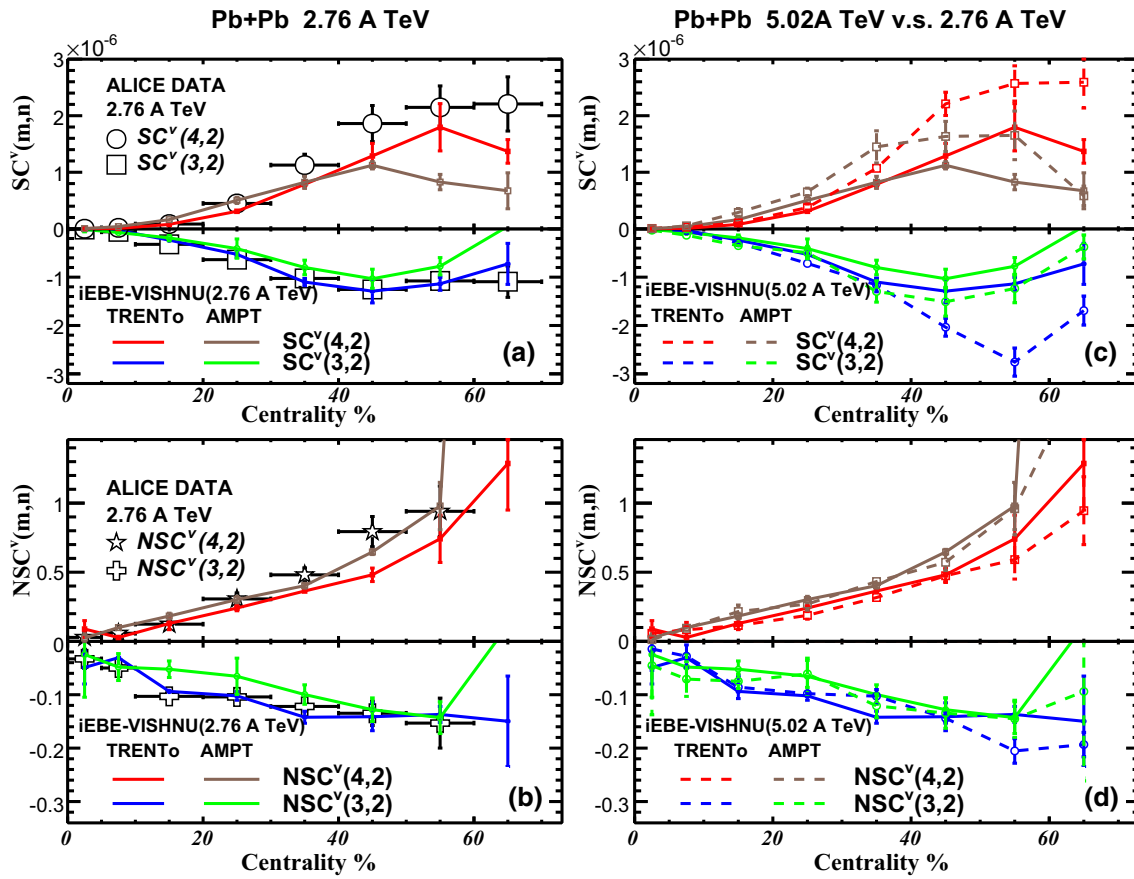


**Fig. 9** Symmetric cumulants  $SC^v(m, n)$  and normalized symmetric cumulants  $NSC^v(m, n)$  in 2.76 and 5.02 A TeV Pb + Pb collisions, calculated from iEBE-VISHNU with TRENTo and AMPT initial condi-

tions. The  $SC^v(3, 2)$  and  $SC^v(4, 2)$  data in 2.76 A TeV Pb + Pb collisions are taken from the ALICE paper [37]

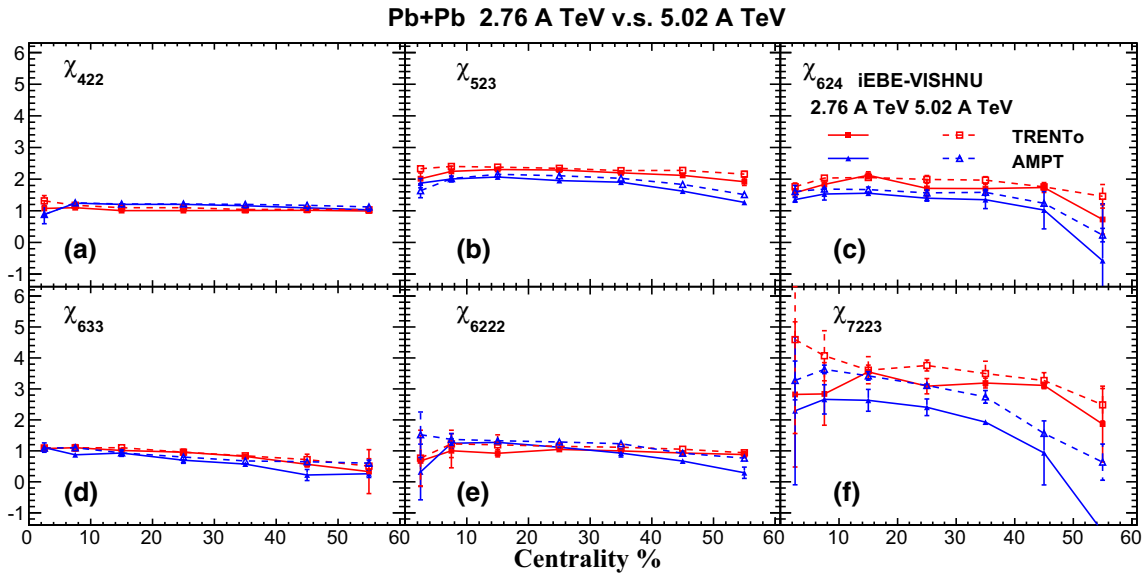


**Fig. 10** iEBE-VISHNU predictions for the centrality dependence of the non-linear response coefficients in 2.76 and 5.02 A TeV Pb + Pb collisions

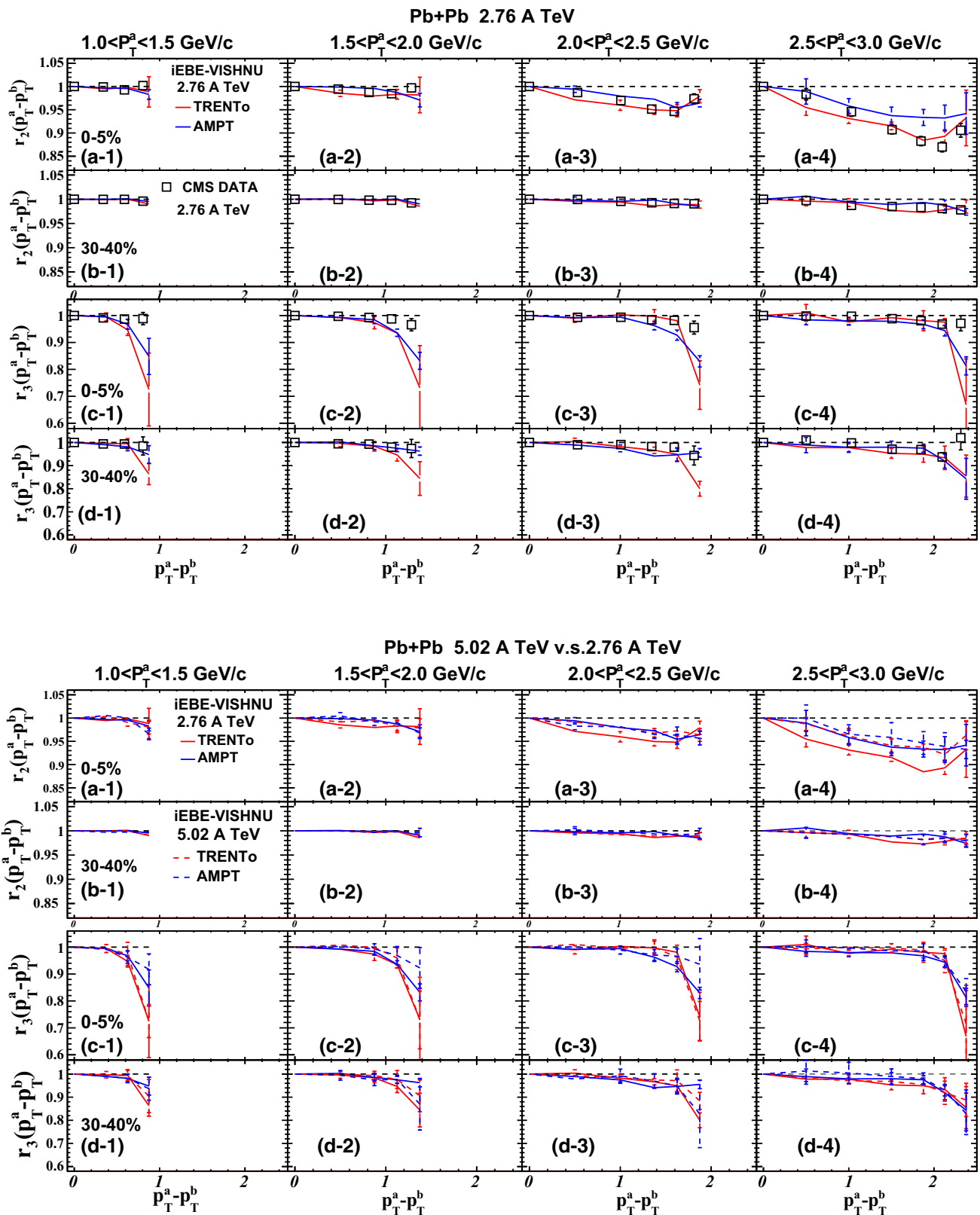


**Fig. 11** The factorization ratio,  $r_2$  and  $r_3$ , as a function of  $p_T^a - p_T^b$  in 0–5 and 30–40% Pb + Pb collisions at 2.76 and 5.02 A TeV, calculated from iEBE-VISHNU with TRENTo and AMPT initial conditions. The experimental data at 2.76 A TeV are taken from the CMS paper [44]

as the event-by-event  $v_n$  distributions [28,86]. Compared with the early investigations, our  $\text{iEBE-VISHNU}$  simulations with  $\text{TRENTO}$  and  $\text{AMPT}$  initial conditions could nicely describe the data of individual flow harmonics, which also largely improve the description of the event-plane correlations. Similarly, the recent  $\text{MUSIC}$  simulations with the successful  $\text{IP-Glasma}$  initial condition also nicely described these measured event-plane correlations [55].

The right panels of Fig. 8 show the  $\text{iEBE-VISHNU}$  predictions on the event-plane correlations in 5.02 A TeV Pb + Pb collisions, which almost overlap with the corresponding ones at 2.76 A TeV. Some of the correlators  $\langle \cos 4(\Psi_2 - \Psi_4) \rangle$ ,  $\langle \cos 6(\Psi_2 - \Psi_6) \rangle$ ,  $\langle \cos(10\Psi_2 - 4\Psi_4 - 6\Psi_6) \rangle$ , etc. show certain separations for  $\text{TRENTO}$  and  $\text{AMPT}$  initial conditions, but are insensitive to the collision energy. This indicates that the hydrodynamic responses of the corresponding initial correlations are similar at these two collision energies.

Figure 9 shows the symmetric cumulants  $\text{SC}^v(4, 2)$  and  $\text{SC}^v(3, 2)$  and normalized symmetric cumulants  $\text{NSC}^v(4, 2)$  and  $\text{NSC}^v(3, 2)$  in Pb + Pb collisions at 2.76 and 5.02 A TeV.<sup>5</sup> Following [37], these symmetric cumulants are calculated by the Q-cumulant method within  $0.2 < p_T < 5.0$  GeV and  $|\eta| < 0.8$ . The left panels compare our model calculations with the experimental data in 2.76 A TeV Pb + Pb collisions. For both  $\text{TRENTO}$  and  $\text{AMPT}$  initial conditions,  $\text{iEBE-VISHNU}$  could roughly describe the centrality-dependent  $\text{SC}^v(m, n)$  and  $\text{NSC}^v(m, n)$ , which also indicate that  $v_2$  and  $v_4$  are correlated and  $v_2$  and  $v_3$  are anti-correlated. In Ref. [87], it was pointed out that both centrality bin width and non-trivial event weighting influence the measured and calculated symmetric cumulants. A quantitative description of the  $\text{SC}(m, n)$  and  $\text{NSC}(m, n)$  data should take these factors into consideration, which we would like to leave to future study.

The right panels of Fig. 9 show the  $\text{iEBE-VISHNU}$  predictions for the symmetric cumulants  $\text{SC}^v(4, 2)$  and  $\text{SC}^v(3, 2)$  and the normalized symmetric cumulants  $\text{NSC}^v(4, 2)$  and  $\text{NSC}^v(3, 2)$  in 5.02 A TeV Pb + Pb collisions. Due to the slightly larger integrated flow harmonics, the absolute values of  $\text{SC}^v(4, 2)$  and  $\text{SC}^v(3, 2)$  also increase from 2.76 to 5.02 A TeV Pb + Pb collisions, while the normalized symmetric cumulant  $\text{NSC}^v(4, 2)$  and  $\text{NSC}^v(3, 2)$  do not significantly change with the collision energy. In [40], it was pointed out that the  $\text{NSC}^v(3, 2)$  is mainly determined by the  $\text{NSC}^e(3, 2)$  from the initial state due to the linear response  $v_2 \propto \varepsilon_2$  and  $v_3 \propto \varepsilon_3$ . Due to the mode coupling between

$v_2$  and  $v_4$ ,  $\text{NSC}^v(4, 2)$  is influenced by both initial conditions and the non-linear evolution of the systems. Here we find that  $\text{NSC}^v(4, 2)$  shows a certain sensitivity to the initial conditions, but it does not significantly change with the collision energy, even though the hydrodynamic evolution time increases.

In Fig. 10, we predict the centrality-dependent non-linear response coefficients in Pb + Pb collisions at 2.76 A TeV and 5.02 A TeV, using  $\text{iEBE-VISHNU}$  hybrid model with  $\text{TRENTO}$  and  $\text{AMPT}$  initial conditions. These non-linear response coefficients are calculated according to the scalar-product formula in Eq. (18) with two sub-events divided by a pseudorapidity gap  $|\Delta\eta| > 0.8$  and within  $0.3 < p_T < 3.0$  GeV and  $|\eta| < 2.4$ . For the collision energies at both 2.76 and 5.02 A TeV, these non-linear response coefficients present weak centrality dependence, except for the  $\chi_{7223}$ . As found in the early paper [80], these non-linear response coefficients exhibit certain sensitivity to the initial condition. For example,  $\chi_{523}$ ,  $\chi_{624}$  and  $\chi_{723}$  show clear separations for  $\text{TRENTO}$  and  $\text{AMPT}$  initial conditions. On the other hand, the non-linear response coefficients, except for  $\chi_{7223}$ , are not sensitive to these two collision energies in our model calculations.

Figure 11 shows the  $p_T$ -dependent factorization ratios,  $r_2$  and  $r_3$ , as a function of  $p_T^a - p_T^b$  in 0–5 and 30–40% Pb + Pb collisions at 2.76 and 5.02 A TeV. Following [44], we calculate the  $p_T$ -factorization ratio,  $r_2$  and  $r_3$ , using the scalar-product method with  $|\eta^{a,b}| < 2.4$  and  $|\Delta\eta| > 2$ . In the upper panels, we compare the  $\text{iEBE-VISHNU}$  results with the CMS data in 2.76 A TeV Pb + Pb collisions. For both  $\text{TRENTO}$  and  $\text{AMPT}$  initial conditions, the  $\text{iEBE-VISHNU}$  hybrid model roughly describes the measured  $r_2(p_T^a, p_T^b)$  data in four bins of  $p_T^a$ . However,  $r_3(p_T^a, p_T^b)$  from  $\text{iEBE-VISHNU}$  drops sharply at larger  $p_T^a - p_T^b$  values, which obviously deviates from the CMS data. In [55], it was pointed out that the hadronic rescatterings during the late evolution randomize the flow angles of  $v_3$ , leading to larger factorization breaking there.

The lower panels show the  $\text{iEBE-VISHNU}$  predictions of  $r_2(p_T^a, p_T^b)$  and  $r_3(p_T^a, p_T^b)$  in 5.02 A TeV Pb + Pb collisions. We found, for both  $\text{TRENTO}$  and  $\text{AMPT}$  initial conditions, that the values of  $r_2$  and  $r_3$  are pretty close for the two collision energies at 2.76 and 5.02 A TeV, which indicates that the non-linear response patterns do not significantly change with the collision energy.

## 5 Summary

In this paper, we studied and predicted various flow observables in Pb + Pb collisions at 2.76 and 5.02 A TeV, using the  $\text{iEBE-VISHNU}$  hybrid model with  $\text{TRENTO}$  and  $\text{AMPT}$  initial conditions and with different forms of the QGP trans-

<sup>5</sup> Other symmetric cumulants  $\text{SC}^v(4, 3)$  and  $\text{SC}^v(5, 2)$  can also be predicted, using the same  $\text{iEBE-VISHNU}$  simulations. However, the related normalized symmetric cumulants  $\text{NSC}^v(4, 3)$  and  $\text{NSC}^v(5, 2)$  require much higher statistical runs to reduce the error bars. Therefore, we do not further predict them here. For related investigations, see [40].

port coefficients. More specifically, we have calculated the integrated and differential flow harmonics of all charged and identified hadrons, the event-by-event  $v_n$  distributions, the event-plane correlations, the correlations between different flow harmonics, the nonlinear response coefficients of higher-order flow harmonics, and  $p_T$ -dependent factorization ratios. A comparison with the flow measurements in 2.76 A TeV Pb + Pb collisions showed that many of these flow observables can be well described by our model calculations with these two chosen initial conditions, as long as the transport coefficients and other related parameters are properly tuned. Some of the flow observables, such as the event-plane correlations  $\langle \cos 4(\Psi_2 - \Psi_4) \rangle$  and  $\langle \cos 6(\Psi_2 - \Psi_6) \rangle$ , the nonlinear response coefficients  $\chi_{624}$  and  $\chi_{723}$ , and so on show certain differences for the results obtained with TRENTO and AMPT initial conditions. A detailed study of these related flow observables in the future may reveal more details of the initial state fluctuation patterns and the non-linear evolution of the systems.

With almost the same parameter sets, except for the retuned normalization factors of initial entropy/energy densities, we predicted various flow observables in 5.02 A TeV Pb + Pb collisions. For the flow harmonics  $v_n$  of all charged hadrons, our iEBE-VISHNU simulations describe the measured data with the same transport coefficients sets. This indicates that raising the collision energy from 2.76 to 5.02 A TeV with the final multiplicities increased by  $\sim 30\%$ , the transport properties of the QGP fireball do not significantly change. We also predicted other flow observables, including  $v_n(p_T)$  of identified particles, event-by-event  $v_n$  distributions, event-plane correlations, (normalized) symmetric cumulants, nonlinear response coefficients and  $p_T$ -dependent factorization ratios, for 5.02 A TeV Pb + Pb collisions. We found that many of these observables approximately keep the same values as the ones in 2.76 A TeV Pb + Pb collisions. Our theoretical investigations and predictions could shed light on the experimental measurements in the near future.

**Acknowledgements** We thank the discussion from A. Behera, J. E. Bernhard, J. Jia, Z. Lin, C. Shen and Y. Zhou. This work is supported by the NSFC and the MOST under Grant nos. 11435001, 11675004 and 2015CB856900. H.X. is partially supported by the China Postdoctoral Science Foundation under Grant no. 2015M580908. We gratefully acknowledge the extensive computing resources provided by the Super-computing Center of Chinese Academy of Science (SCCAS) and Tianhe-1A from the National Supercomputing Center in Tianjin, China.

**Open Access** This article is distributed under the terms of the Creative Commons Attribution 4.0 International License (<http://creativecommons.org/licenses/by/4.0/>), which permits unrestricted use, distribution, and reproduction in any medium, provided you give appropriate credit to the original author(s) and the source, provide a link to the Creative Commons license, and indicate if changes were made. Funded by SCOAP<sup>3</sup>.

## References

1. I. Arsene et al., (BRAHMS Collaboration), Nucl. Phys. A **757**, 1 (2005)
2. B. B. Back et al., (PHOBOS Collaboration), *ibid.*, p. 28
3. J. Adams et al., (STAR Collaboration), *ibid.*, p. 102
4. K. Adcox et al., (PHENIX Collaboration), *ibid.*, p. 184
5. M. Gyulassy, in *Structure and dynamics of elementary matter. NATO science series II: Mathematics, physics and chemistry*, vol. 166 ed. by W. Greiner et al., (Kluwer Academic, Dordrecht, 2004), pp. 159–182
6. M. Gyulassy, L. McLerran, Nucl. Phys. A **750**, 30 (2005)
7. E. V. Shuryak, *ibid.*, p. 64
8. B. Muller, J.L. Nagle, Ann. Rev. Nucl. Part. Sci. **56**, 93 (2006)
9. B. Muller, J. Schukraft, B. Wyslouch, Ann. Rev. Nucl. Part. Sci. **62**, 361 (2012)
10. D.A. Teaney, [arXiv:0905.2433](https://arxiv.org/abs/0905.2433) [nucl-th]
11. P. Romatschke, Int. J. Mod. Phys. E **19**, 1 (2010)
12. P. Huovinen, Int. J. Mod. Phys. E **22**, 1330029 (2013)
13. U. Heinz, R. Snellings, Ann. Rev. Nucl. Part. Sci. **63**, 123 (2013)
14. C. Gale, S. Jeon, B. Schenke, Int. J. Mod. Phys. A **28**, 1340011 (2013)
15. H. Song, Y. Zhou, K. Gajdosova, [arXiv:1703.00670](https://arxiv.org/abs/1703.00670) [nucl-th]
16. H. Song, Pramana **84**, 703 (2015)
17. H. Song, Nucl. Phys. A **904–905**, 114c (2013)
18. M. Luzum, H. Petersen, J. Phys. G **41**, 063102 (2014)
19. J. Jia, J. Phys. G **41**(12), 124003 (2014)
20. K. Aamodt et al., [ALICE Collaboration], Phys. Rev. Lett. **107**, 032301 (2011)
21. G. Aad et al., [ATLAS Collaboration], Phys. Rev. C **86**, 014907 (2012)
22. B.H. Alver, C. Gombeaud, M. Luzum, J.Y. Ollitrault, Phys. Rev. C **82**, 034913 (2010)
23. F.G. Gardim, F. Grassi, M. Luzum, J.Y. Ollitrault, Phys. Rev. C **85**, 024908 (2012)
24. H. Song, S.A. Bass, U. Heinz, Phys. Rev. C **83**, 054912 (2011)
25. H. Song, S. Bass, U.W. Heinz, Phys. Rev. C **89**(3), 034919 (2014)
26. H.j Xu, Z. Li, H. Song, Phys. Rev. C **93**(6), 064905 (2016)
27. C. Gale, S. Jeon, B. Schenke, P. Tribedy, R. Venugopalan, Phys. Rev. Lett. **110**(1), 012302 (2013)
28. G. Aad et al., [ATLAS Collaboration], JHEP **1311**, 183 (2013)
29. L. Yan, J.Y. Ollitrault, A.M. Poskanzer, Phys. Rev. C **90**(2), 024903 (2014)
30. Y. Zhou, K. Xiao, Z. Feng, F. Liu, R. Snellings, Phys. Rev. C **93**(3), 034909 (2016)
31. G. Aad et al., [ATLAS Collaboration], Phys. Rev. C **90**(2), 024905 (2014)
32. Z. Qiu, U. Heinz, Phys. Lett. B **717**, 261 (2012)
33. R.S. Bhalerao, J.Y. Ollitrault, S. Pal, Phys. Rev. C **88**, 024909 (2013)
34. D. Teaney, L. Yan, Phys. Rev. C **90**(2), 024902 (2014)
35. R.S. Bhalerao, J.Y. Ollitrault, S. Pal, Phys. Lett. B **742**, 94 (2015)
36. G. Aad et al., [ATLAS Collaboration], Phys. Rev. C **92**(3), 034903 (2015)
37. J. Adam et al., [ALICE Collaboration], Phys. Rev. Lett. **117**, 182301 (2016)
38. H. Niemi, K.J. Eskola, R. Paatelainen, Phys. Rev. C **93**(2), 024907 (2016)
39. G. Giacalone, L. Yan, J. Noronha-Hostler, J.Y. Ollitrault, Phys. Rev. C **94**(1), 014906 (2016)
40. X. Zhu, Y. Zhou, H. Xu, H. Song, [arXiv:1608.05305](https://arxiv.org/abs/1608.05305) [nucl-th]
41. J. Qian, U. Heinz, Phys. Rev. C **94**(2), 024910 (2016)
42. U. Heinz, Z. Qiu, C. Shen, Phys. Rev. C **87**(3), 034913 (2013)
43. F.G. Gardim, F. Grassi, M. Luzum, J.Y. Ollitrault, Phys. Rev. C **87**(3), 031901 (2013)

44. V. Khachatryan et al., [CMS Collaboration], *Phys. Rev. C* **92**(3), 034911 (2015)
45. Y. Zhou, [ALICE Collaboration], *Nucl. Phys. A* **931**, 949 (2014)
46. L.G. Pang, G.Y. Qin, V. Roy, X.N. Wang, G.L. Ma, *Phys. Rev. C* **91**(4), 044904 (2015)
47. L.G. Pang, H. Petersen, G.Y. Qin, V. Roy, X.N. Wang, *Eur. Phys. J. A* **52**(4), 97 (2016)
48. K. Xiao, L. Yi, F. Liu, F. Wang, *Phys. Rev. C* **94**(2), 024905 (2016)
49. G.L. Ma, Z.W. Lin, *Phys. Rev. C* **93**(5), 054911 (2016)
50. J.S. Moreland, J.E. Bernhard, S.A. Bass, *Phys. Rev. C* **92**(1), 011901 (2015)
51. J.E. Bernhard, J.S. Moreland, S.A. Bass, J. Liu, U. Heinz, *Phys. Rev. C* **94**(2), 024907 (2016)
52. J. Adam et al., [ALICE Collaboration], *Phys. Rev. Lett.* **116**(13), 132302 (2016)
53. H. Niemi, K.J. Eskola, R. Paatelainen, K. Tuominen, *Phys. Rev. C* **93**(1), 014912 (2016)
54. J. Noronha-Hostler, M. Luzum, J.Y. Ollitrault, *Phys. Rev. C* **93**(3), 034912 (2016)
55. S. McDonald, C. Shen, F. Fillion-Gourdeau, S. Jeon, C. Gale, [arXiv:1609.02958](https://arxiv.org/abs/1609.02958) [hep-ph]
56. C. Shen, Z. Qiu, H. Song, J. Bernhard, S. Bass, U. Heinz, *Comput. Phys. Commun.* **199**, 61 (2016)
57. H. Song, S.A. Bass, U. Heinz, *Phys. Rev. C* **83**, 024912 (2011)
58. H. Song, U.W. Heinz, *Phys. Lett. B* **658**, 279 (2008)
59. H. Song, U.W. Heinz, *Phys. Rev. C* **77**, 064901 (2008)
60. H. Song, Ph.D Thesis, The Ohio State University (2009), [arXiv:0908.3656](https://arxiv.org/abs/0908.3656) [nucl-th]
61. M. Bleicher et al., *J. Phys. G* **25**, 1859 (1999)
62. S.A. Bass et al., *Prog. Part. Nucl. Phys.* **41**, 255 (1998)
63. J.D. Bjorken, *Phys. Rev. D* **27**, 140 (1983)
64. U.W. Heinz, H. Song, A.K. Chaudhuri, *Phys. Rev. C* **73**, 034904 (2006)
65. A. Bazavov et al., [HotQCD Collaboration], *Phys. Rev. D* **90**, 094503 (2014)
66. K. Dusling, T. Schffer, *Phys. Rev. C* **85**, 044909 (2012)
67. J. Noronha-Hostler, G.S. Denicol, J. Noronha, R.P.G. Andrade, F. Grassi, *Phys. Rev. C* **88**(4), 044916 (2013)
68. R.S. Bhalerao, A. Jaiswal, S. Pal, *Phys. Rev. C* **92**(1), 014903 (2015)
69. L. Pang, Q. Wang, X.N. Wang, *Phys. Rev. C* **86**, 024911 (2012)
70. Y. Zhou, *Adv. High Energy Phys.* **2016**, 9365637 (2016)
71. K. Aamodt et al., [ALICE Collaboration], *Phys. Rev. Lett.* **106**, 032301 (2011)
72. J. Adam et al., [ALICE Collaboration], *Phys. Rev. Lett.* **116**(22), 222302 (2016)
73. S. Voloshin, Y. Zhang, *Z. Phys. C* **70**, 665 (1996)
74. A. Bilandzic, R. Snellings, S. Voloshin, *Phys. Rev. C* **83**, 044913 (2011)
75. Y. Zhou, X. Zhu, P. Li, H. Song, *Phys. Rev. C* **91**, 064908 (2015)
76. H.-j. Xu, H. Song, unpublished notes
77. J. Jia, S. Mohapatra, *Phys. Rev. C* **88**(1), 014907 (2013)
78. T. Abye, [arXiv:1105.1160](https://arxiv.org/abs/1105.1160) [physics.data-an]
79. Z.W. Lin, C.M. Ko, B.A. Li, B. Zhang, S. Pal, *Phys. Rev. C* **72**, 064901 (2005)
80. J. Qian, U.W. Heinz, J. Liu, *Phys. Rev. C* **93**(6), 064901 (2016)
81. L. Yan, J.Y. Ollitrault, *Phys. Lett. B* **744**, 82 (2015)
82. B. Abelev et al., [ALICE Collaboration], *Phys. Rev. C* **88**, 044910 (2013)
83. J. Adam et al., [ALICE Collaboration], *JHEP* **1609**, 164 (2016)
84. R. Snellings, *EPJ Web Conf.* **97**, 00025 (2015)
85. U.W. Heinz, J. Liu, *Nucl. Phys. A* **956**, 549 (2016)
86. C. Shen, Ph.D Thesis, The Ohio State University (2014), The standard model for relativistic heavy-ion collisions and electromagnetic tomography
87. F.G. Gardim, F. Grassi, M. Luzum, J. Noronha-Hostler, *Phys. Rev. C* **95**(3), 034901 (2017)